LA-UR-16-20140
Approved for public release; distribution is unlimited.

Title: Barrier experiment: Shock initiation under complex loading

Author(s): Menikoff, Ralph

Intended for: Report

Issued: 2016-01-12

Barrier experiment: Shock initiation under complex loading

Ralph Menikoff

December 20, 2015

Abstract

The barrier experiments are a variant of the gap test; a detonation wave in a donor HE impacts a barrier and drives a shock wave into an acceptor HE. The question we ask is: What is the trade-off between the barrier material and threshold barrier thickness to prevent the acceptor from detonating. This can be viewed from the perspective of shock initiation of the acceptor subject to a complex pressure drive condition. Here we consider key factors which affect whether or not the acceptor undergoes a shock-to-detonation transition. These include the following: shock impedance matches for the donor detonation wave into the barrier and then the barrier shock into the acceptor, the pressure gradient behind the donor detonation wave, and the curvature of detonation front in the donor. Numerical simulations are used to illustrate how these factors affect the reaction in the acceptor.

1 Introduction

For the gap test, see for example [Gibbs and Popolato, 1980, Part II, sec. 4.2], a detonation wave in a donor HE impacts a barrier and drives a shock wave into an acceptor HE. The threshold barrier thickness for the acceptor to detonate is a measure of the relative sensitivity of the acceptor HE. Due to the complex loading, the measured sensitivity depends on the drive condition that the acceptor is subjected to. As a result, there are many variants of the gap test based on the donor HE, test geometry (diameter of the HE and confinement), and barrier material.

The barrier experiments utilized PBX 9502 for both the donor and acceptor HE. They are aimed at determining the trade-off between the barrier material and its threshold thickness. The experiments used two geometries: cylindrical [Francois and Scovel, 2014] and slab [Dattelbaum et al., 2015]. The slab geometry was used in order to obtain proton radiography images of the flow. There is a significant difference in barrier threshold thickness for the two geometries.

Here we discuss four key factors which affect whether the acceptor undergoes a shock-to-detonation transition(SDT). First is the shock impedance matches of the donor detonation wave into the barrier and then the barrier shock into the acceptor. Second is the pressure gradient behind the donor detonation wave which causes the lead shock in the barrier to decay, and in turn gives rise to a pressure gradient behind the lead shock in the acceptor. Third is the curvature of the lead shock front which also affects the decay of the shock. Fourth is the reaction in the acceptor. The competition between the reaction and the other factors determines whether the lead shock in the acceptor builds up to a detonation or decays.

Numerical simulations with an epoxy barrier are used to compute the flow in the acceptor for several cases. An inert acceptor (EOS of reactants but without reaction) is used to determine how fast the lead shock in the acceptor would decay from the non-reaction factors. Then simulations with a burn model for the cylindrical case show examples with the barrier thickness just above and just below the threshold. For the slab case, simulations with an inert acceptor show that the decay of the lead shock is much slower than for the cylindrical case. This is mostly due to the difference in the pressure gradient behind the donor detonation wave.

2 Shock initiation

Here we briefly discuss factors that affect a shock-to-detonation transition for the complex loading of the barrier experiment.

2.1 Pop plot

A key characterization of shock initiation is the Pop plot [see Gibbs and Popolato, 1980, Part II, sec. 4.1]; distance-of-run to detonation vs shock pressure on a log-log plot. It is based on data from experiments in which the HE is driven by a sustained shock and the flow is one-dimensional. For more complicated drive conditions, it sets the scale for how long the drive pressure must be maintained for a SDT to occur.

The Pop plot for PBX 9502 is shown in figure 1. The data for initial shock pressure is in the range from 8 to 15 GPa. Above 15 GPa, initiation occurs promptly; within a couple of mm. Below 8 GPa, an SDT does not occur within the length of the HE sample used in experiments. Partly, for sample lengths greater than 30 or 40 mm, it is difficult to maintain 1-D flow due to rarefaction waves from the sides or back. In addition, below 8 GPa, the hot spot rate is very low. We will take 8 GPa as a threshold pressure for shock initiation to occur.

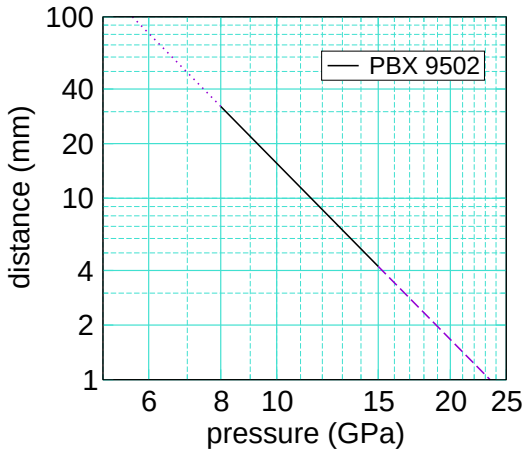

Figure 1: Pop plot for PBX 9502. Solid line is fit to data. Dash line is extension to high pressure. Detonation wave typically fails for low pressure, dotted line.

For the barrier experiments, to prevent the acceptor from detonating, the pressure gradient behind the initial shock needs to cause the lead shock in the acceptor to decay below the initiation threshold pressure in a distance comparable to or less than the run distance on the Pop plot for the initial acceptor shock pressure. The decay distance can be larger if the lead front is curved and the shock wave is diverging.

2.2 Impedance match

The initial shock pressure in the acceptor can be estimated from the impedance matches of the donor detonation wave into the barrier and then the barrier shock into the acceptor. The ZND wave profile of a detonation consists of a shock in the reactants to the von Neumann spike state and then a pressure decrease in the reaction zone to the CJ pressure in the products. Since the reaction zone is narrow, the pressure gradient in the reaction zone is very large, and its affect on the transmitted wave in the barrier would decay very rapidly. Therefore, for the impedance match with the detonation wave we neglect the reaction zone and use the detonation state in the products. For the second impedance match of the barrier shock into the acceptor we neglect the effect of the pressure gradient behind the detonation wave which would cause the barrier shock to decay. Thus, the impedance match gives an overestimate of the initial shock pressure in the acceptor. It is useful in estimating the relative effect of different barrier materials.

Figure 2 shows the graphical solutions in the particle velocity-pressure plane, (u, P)-plane, of the impedance matches for an epoxy barrier. For the first match, detonation wave into the epoxy, the pressure goes down. Then for the second match, the pressure in the acceptor goes up to slightly less than the CJ pressure. In this case, the pressure gradient behind the detonation wave will play a crucial role on whether or not the acceptor detonates.

Two other barrier materials illustrate the range of behavior for the impedance matches; tantalum and polyurea aerogel [Aslam et al., 2014]. Tantalum has a high density and consequently a high acoustic impedance. This results in a large slope for the wave curves in the (u, P)-plane; as the impedance matches in figure 3 show. The first shock has a pressure much higher than the CJ pressure, but the match into the acceptor gives a much lower pressure, about 12 GPa. Though much lower than for the epoxy barrier, the initial acceptor shock pressure is still in the range of a SDT. Hence, the pressure

gradient behind the detonation wave would still be important for initiation to fail in the acceptor.

Aerogels can have a very high porosity. The impedance match for a polyurea aerogel with 82 % porosity is shown in figure 4. Due to the low density of the aerogel, the first match results in low pressure, about 5 GPa. The second match gives a shock pressure in the acceptor of about 16 GPa, significant less than for the epoxy barrier.

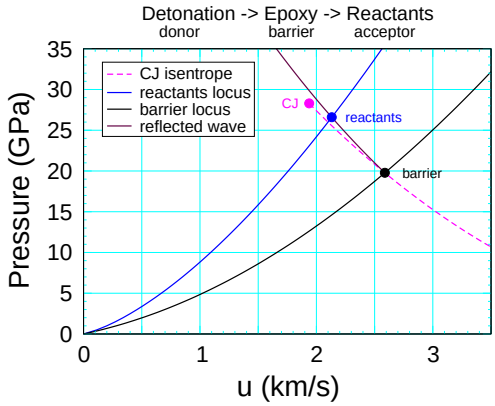

Figure 2: Impedance matches for detonation wave into epoxy barrier and then epoxy shock into acceptor. The symbols corresponds to the match states; magenta for the detonation wave, black for barrier shock and blue for acceptor shock.

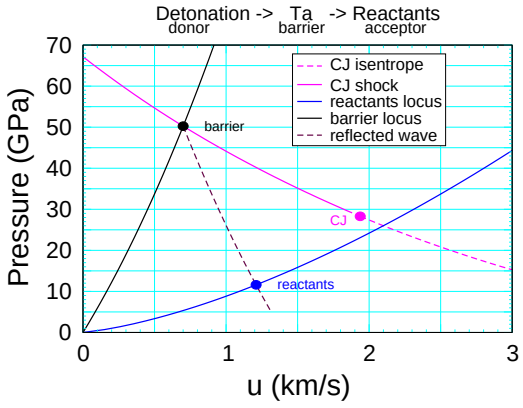

Figure 3: Impedance matches for detonation wave into Ta barrier and then Ta shock into acceptor. The symbols corresponds to the match states; magenta for the detonation wave, black for barrier shock and blue for acceptor shock.

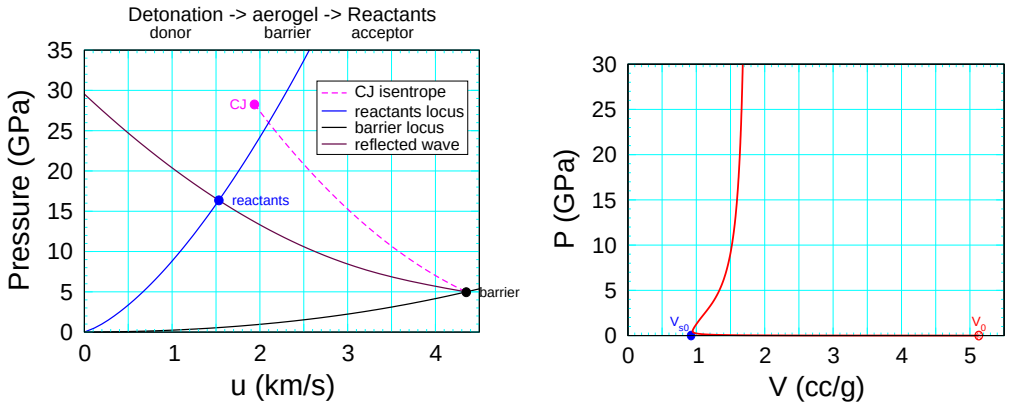

Figure 4: Impedance matches for detonation wave into polyurea aerogel barrier with 82 % porosity and then aerogel shock into acceptor. The symbols corresponds to the match states; magenta for the detonation wave, black for barrier shock and blue for acceptor shock. Right plot is aerogel shock locus in the (V, P)-plane. Symbols labeled V_0 and V_{s0} correspond to the specific volume of the initial aerogel and the solid polyurea, respectively.

Typical, a foam or porous plastic would compress to a density higher than the normal solid density. This would result in the reflected shock locus having a slope in the (u, P)-plane similar to that of the shocked solid. Moreover, the slope for polymers are similar to that of epoxy. Consequently, low to moderate porosity would result in the first match having a lower pressure on the HE products rarefaction curve, but the second match would give about the same pressure as a barrier of the same material without porosity. This would be about the same pressure as for the epoxy that is shown in figure 2.

What makes the aerogel different is that the very high porosity results in a very large amount of shock heating. The shock heating results in a high temperature that causes the polyurea to decompose and expand. Consequently, the shock locus in the (V, P)-plane compresses to near solid density at a low shock pressure and then expands as the shock pressure increases, as shown in figure 4. The low shock density for the first impedance match results in the reflected shock locus having a lower slope in the (u, P)-plane than that of the normal solid. The difference in the slopes of the reflected shock locus for the barrier and the products release isentrope is what leads to a lower shock pressure in the acceptor.

2.3 Shock strength

The flow behind a shock front is subsonic and can cause the shock speed to either accelerate or de-accelerate. The change in the shock strength is determined by the forward characteristic impinging on the shock front from behind the wave. For a right facing wave, the characteristic equation is expressed in terms of the right Riemann invariant $\mathcal{R}^+$ defined by $\mathsf{d}\mathcal{R}^+ = \mathsf{d}P + \rho\, c\, \mathsf{d}u$:

$$[\partial_t + (u+c)\partial_x]\,\mathcal{R}^+ = (\partial_\lambda P)_{V,e}\mathsf{R} - \rho\, c^2\, u\, \partial_x A/A \ , \tag{1}$$

where λ is the reaction progress variable (mass fraction of the products), c is the frozen sound speed (fixed λ), e is the specific internal energy, R is the reaction rate and A is the cross-sectional area of streak tube for neighboring particles along the shock front. The factor $\partial_x A/A$ is proportional to the mean curvature of the shock front. It is positive for a diverging wave and negative for a converging wave.

The left hand side of Eq. (1) can be expressed as

$$[\partial_t + (u+c)\partial_x]\,\mathcal{R}^+ = [\partial_t + u_s\partial_x]\,\mathcal{R}^+ + (u+c-u_s)\partial_x\mathcal{R}^+ \ ,$$

where u_s is the shock velocity. At the shock front

$$(\mathsf{d}/\mathsf{d}t)\,\mathcal{R}_s^+ = [\partial_t + u_s\partial_x]\,\mathcal{R}^+ \ .$$

Substituting into Eq. (1) yields the shock change equation

$$(\mathsf{d}/\mathsf{d}t)\,\mathcal{R}_s^+ = -(u+c-u_s)\partial_x\mathcal{R}^+ + (\partial_\lambda P)_{V,e}\mathsf{R} - \rho\, c^2\, u\, \partial_x A/A \ . \tag{2}$$

On the shock locus P and u are monotonic. Consequently, $\mathcal{R}_s^+$ increases with shock strength and is a measure of the shock pressure.

For a planar inert shock, only the term $\partial_x\mathcal{R}^+ = \partial_x P + \rho c\, \partial_x u$ contributes to the change in shock strength. Typically, $\partial_x P$ and $\partial_x u$ have the same sign. In addition, one-dimensional shock stability requires that the state behind the shock front is subsonic; *i.e.*, $u + c - u_s > 0$. It follow that a shock strengthens if followed by a compressive wave, $\partial_x P < 0$, and decays if followed by a rarefaction, $\partial_x P > 0$.

For an explosive, $\mathsf{R} \geq 0$ and $\partial_\lambda P > 0$. Consequently, the reaction term is always positive or zero, and strengthens the shock. Since R increases with

pressure, strengthening the lead shock provides positive feedback that leads to a shock-to-detonation transition. For a propagating detonation wave, the cancellation of the reaction term and the pressure gradient term allow for a steady state ZND profile.

The area term on the right hand side of Eq. (2) is important for a curved shock front. In particular, a diverging shock weakens and a converging shock strengthens. This is a requirement for shock stability.

The cumulative effect of the three terms (pressure gradient, reaction rate and front curvature) determines whether the shock strength increases or decreases. Typically, for a shock-to-detonation transition, there is an induction like regime in which the lead shock accelerates slowly. At some point the rate term in Eq. (2) dominates, and the positive feedback with shock acceleration results in a rapid transition to a detonation wave.

We note that the shock change equation (2) with only the area term is the basis for Whitham's shock dynamics [Whitham, 1974, chpt. 8], and with the rate term plus the Pop plot is the basis for the analysis [Menikoff and Shaw, 2008, sec. 5] used to determine the Forest Fire burn rate.

2.4 Simulations

Numerical simulations are needed to account for the decay of the lead shock in the barrier and then the competition between factors that strengthen or weaken the lead shock in the acceptor. In the next sections, results are shown for simulations using the SURF burn model [Menikoff and Shaw, 2010] in the xRage code. Other simulations with the Forest Fire burn model [Mader, 2007] by C. Scovel in the xRage code and E. Moro in the Pagosa code give similar results. Both the xRage and Pagosa codes use an Eulerian mesh.

The burn rate for the SURF model is a function of the lead shock pressure. Since the reaction turns on only after the shock is detected, it can capture the von Neumann spike state of a propagating detonation wave even when the reaction zone is not well resolved. In contrast, the Forest Fire rate is a function of the local pressure. It is not intended to resolve the reaction zone, but aims for a reactive shock profile in which reaction occurs in the shock rise and the von Neumann spike pressure is clipped.

In addition, the SURF model utilizes an algorithm to detect the lead shock. Plotting the lead shock pressure is helpful for understanding the factors that contribute to a shock-to-detonation transition.

3 Cylinder – rate stick

The barrier experiment in cylindrical geometry is similar to a rate stick. The donor, barrier and acceptor are 1 inch in diameter and confined by a lexan tube with $\frac{1}{4}$ inch thick wall. A detonator and 1 inch long PBX 9501 booster is used to initiate the donor. PBX 9502 are used for both the donor and acceptor. Their lengths are 5 and 6 inches, respectively.

The cylindrical barrier simulations presented in this section were meant to compare with simulations using the Pagosa code. A fixed mesh with 0.1 mm cell size is used. For the 9502, a JWL EOS for the products and a Mie-Grünisen EOS for the reactants were used.

Prior to impact with the barrier, the shape of the detonation front and the radial expansion of the lexan tube are seen in the 2-D density plot of figure 5. The pressure and burn fraction profiles along the axis are also shown in figure 5. The pressure gradient behind the detonation front is set by the radial expansion of the wall. The pressure falls below the 8 GPa ignition shock threshold on the Pop plot after slightly under 15 mm. Due to the radial expansion of the wall and the curvature of the detonation front, the pressure profile is largest on the axis. Consequently, if the acceptor detonates, the ignition point will be on the axis.

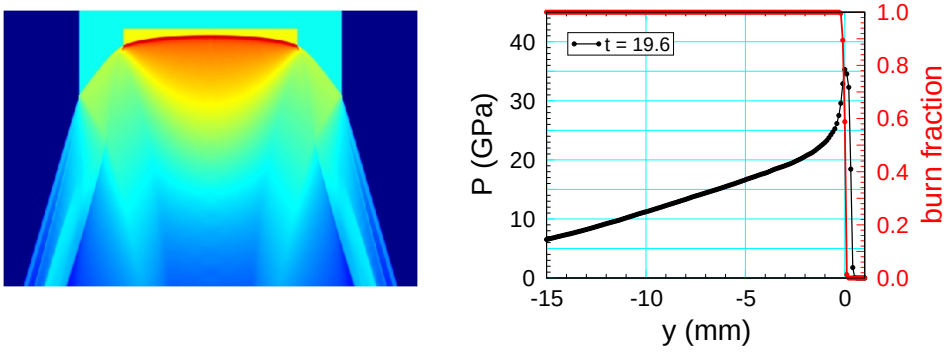

Figure 5: Detonation wave in donor just before impact with barrier. Two-dimensional density plot on left. Detonation wave is propagating up. Note, lexan tube and epoxy barrier have nearly the same density, and are not distinguishable in the plot. Profiles along axis of pressure and burn fraction on the right plot.

3.1 Inert acceptor

To understand the pressure that is driving the acceptor, it is helpful to start with a simulation utilizing an inert acceptor; *i.e.*, an inert material with the EOS of the reactants. Here we use a 10 mm thick epoxy barrier. In the simulation the barrier is initially in the region $152 < y < 162$ mm.

Figure 6 shows the evolution of the pressure profile on axis. The first profile ($t = 19.7$) shows the detonation wave in the donor. It then matches into epoxy sending a reflected rarefaction into the donor. The initial match is from the VN spike state. By $t = 20.1$, the effect of the reaction zone has decayed and the epoxy pressure is close to that of the shock match shown in figure 2. Due to the release wave behind the detonation front, figure 5, the epoxy shock pressure decays to about 12 GPa just before impacting the acceptor. This effect is missing from the second shock match shown in figure 2. The shock match into the acceptor increases the shock pressure to about 15 GPa. The acceptor shock then decays due to the pressure gradient.

The shock pressure as the lead wave propagates through the epoxy barrier and into the acceptor is shown in Figure 7. About 10 mm after the end of the barrier, the acceptor shock pressure is below the shock threshold on the Pop plot.

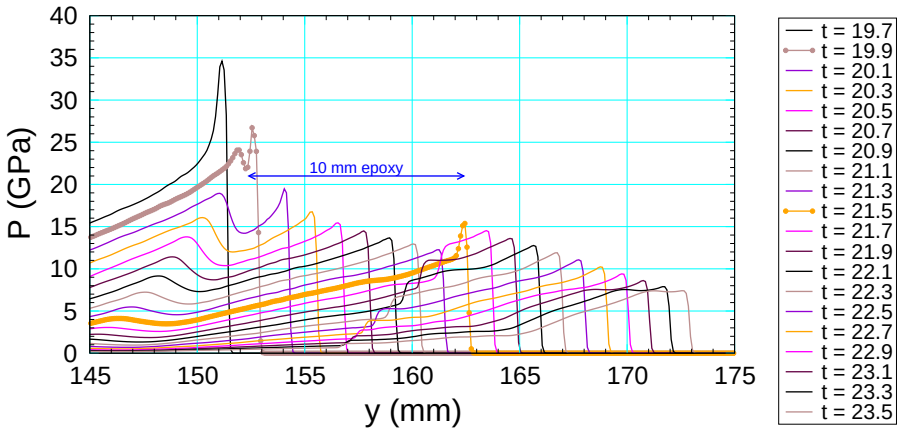

Figure 6: Evolution of pressure profiles on axis for inert acceptor with 10 mm epoxy barrier. Simulation times in μs are in the legend on the right. Brown and orange profiles with symbols are just after shock match of donor detonation into epoxy and epoxy shock into acceptor, respectively. Symbols indicate mesh cells.

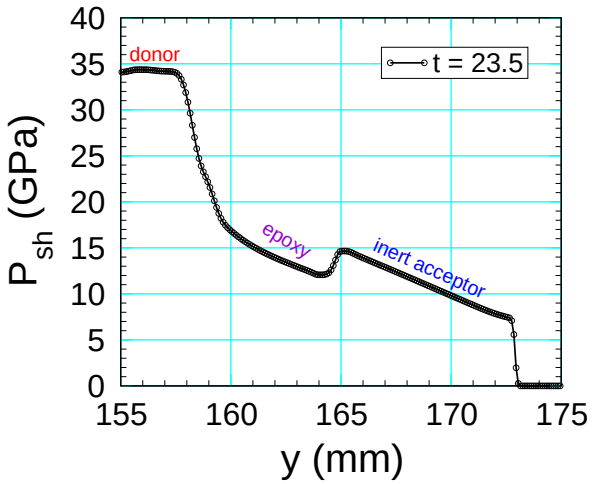

Figure 7: Pressure of lead shock (advected) for inert acceptor with 10 mm epoxy barrier.

3.2 Acceptor detonating

The next simulation is again with the 10 mm epoxy barrier but this time with reaction in the acceptor. A sequence of plots with profiles on axis of the pressure, burn fraction and lead shock pressure are shown in figure 8. The aim is to see how the reaction affects the strength of the lead shock and the feedback of the lead shock strength on the reaction.

The initial shock pressure in the acceptor is about 15 GPa, This is high enough to trigger prompt reaction. The reaction raises the pressure. This is sufficient to reverse the sign of the pressure gradient immediately behind the shock front. Consequently, the shock pressure increase. This in turn increase the rate of reaction. The positive feedback leads to a transition to detonation. The transition occurs at $t = 22.8$, about 8 mm downstream of the epoxy. The run distance to detonation is about double the value on the Pop plot for the initial shock pressure in the acceptor; slightly over 4 mm at 15 GPa.

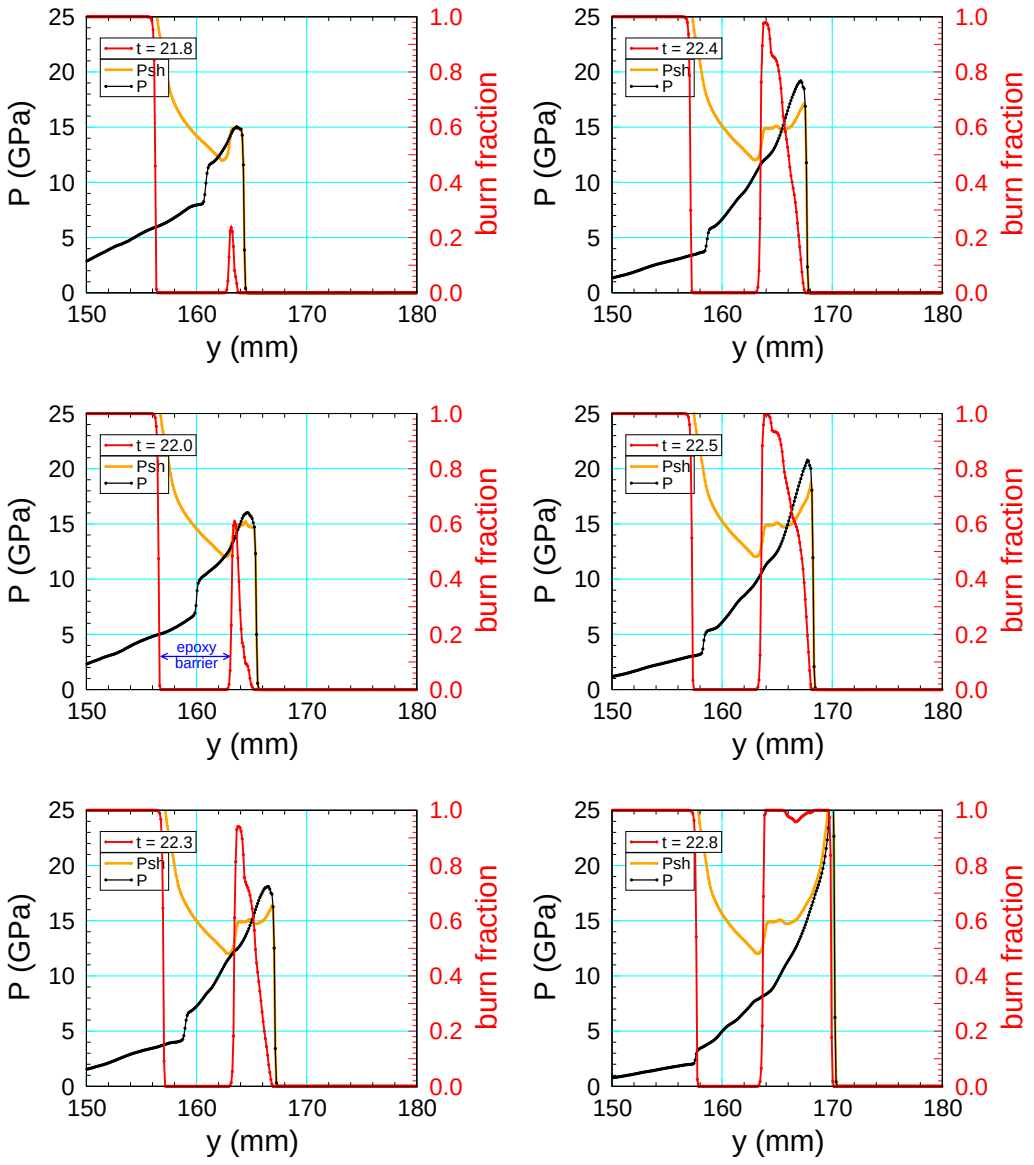

Figure 8: Barrier experiment with 10 mm epoxy barrier; time evolution of profiles on axis for pressure, reaction and lead shock pressure. The gap between reacting regions corresponds to the epoxy barrier.

3.3 Acceptor not detonating

To illustrate the sensitivity on initiation of the competing factors, the next case is with a slightly longer barrier; 11.6 mm epoxy. A sequence of plots with profiles on axis of the pressure, burn fraction and lead shock pressure are shown in figure 10. The initial shock pressure into the acceptor is about 13.5 GPa, and the shock pressure falls below 10 GPa after about 15 mm of run.

The initial reaction again results in a slightly negative pressure gradient behind the lead shock. However, the plots at $t = 22.9$ and $t = 23.4$ show that the shock strength decreases. This is due to two-dimensional effects. Two-dimensional plots of selected fields are shown in figure 11. Reaction on the axis causes the shock front to bow out resulting in a diverging shock wave. The front is significantly more curved than the donor detonation front shown in figure 5. In this case the effect of divergence overcomes the effect of the pressure gradient. The decreasing shock pressure decreases the reaction rate and allows enough time for the release wave behind the donor detonation wave to catch up with the front. Later in time, figure 9, a detonation has clearly failed to develop. Though 25 mm of the acceptor following the barrier is seen to have burned.

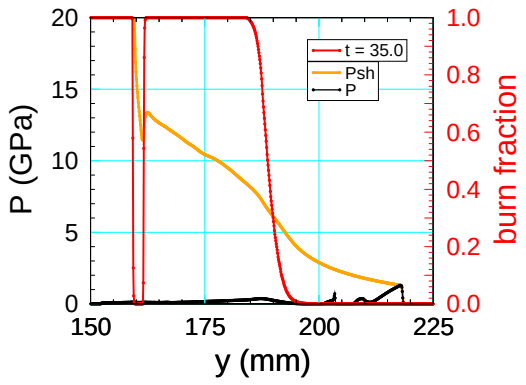

Figure 9: Barrier experiment with 11.6 mm epoxy barrier; profiles on axis for pressure, reaction and lead shock pressure at end of run.

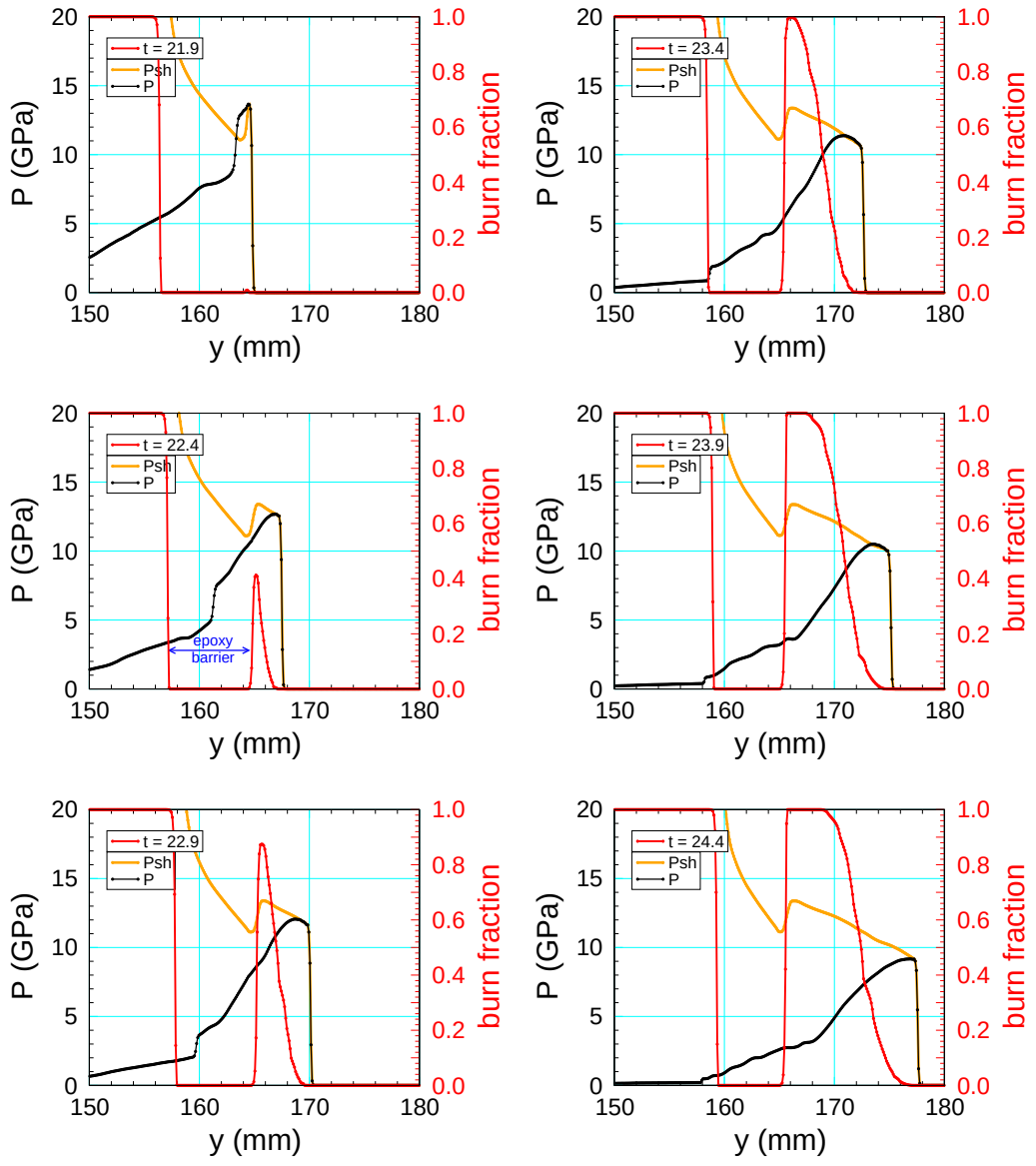

Figure 10: Barrier experiment with 11.6 mm epoxy barrier; time evolution of profiles on axis for pressure, reaction and lead shock pressure. The gap between reacting regions corresponds to the epoxy barrier.

density

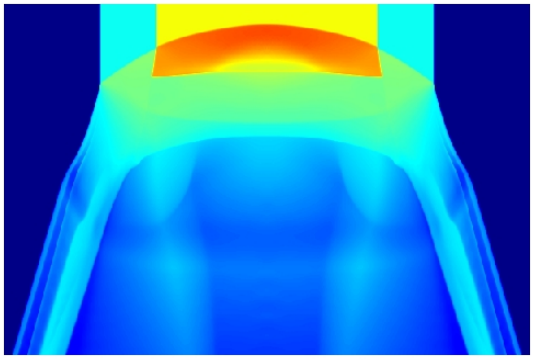

log(pressure)

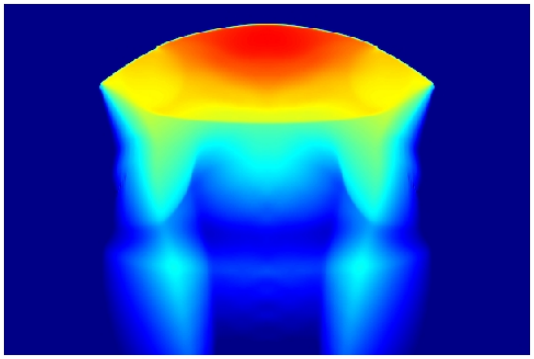

volume fraction
9502 products

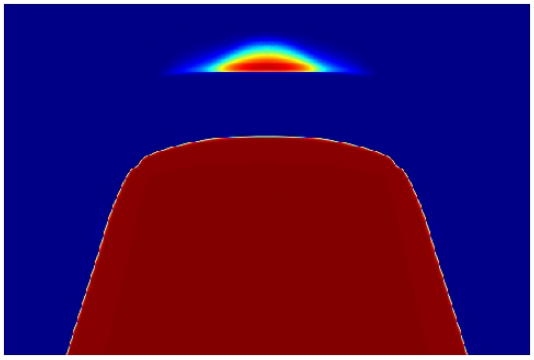

Figure 11: Barrier experiment with 11.6 mm epoxy barrier; 2-D plots of selected variables at $t = 23\,\mu$s.

4 Slab – pRad geometry

The pRad barrier experiments are in slab geometry. The simulations presented in this section will be in planar two-dimensional geometry; *i.e.*, edge effects from the finite width of the slab are neglected. The HE and barrier are 25 mm thick and confined by a sylgard potting layer and tantalum plates. The potting avoids gaps between the tantalum plates and the HE. The assembly is composed of a line wave initiator, 25 mm PBX 9501 booster, 70 mm donor HE and 50 mm acceptor HE. Again PBX 9502 is used for both the donor and acceptor.

The inert layers surrounding the HE give rise to a more complex wave structure impacting the barrier. The experiments used a 0.5 mm sylgard layers and 3 mm tantalum plates. For this case, the 2-D density plot in figure 12 shows the detonation wave just prior to impact with the acceptor. We note that the detonation front is curved and there are oblique waves from shock reflections off the inert layers confining the HE.

Due to the oblique waves, pressure profiles behind the front vary with the distance to the centerline. In addition, the pressure profiles vary with the thickness of the confining layers. The variations are shown in figure 13. The profiles display several characteristic features that reflect the 2-D wave structure: pressure spike from the reaction zone, release rarefaction behind the detonation wave, secondary shock (*e.g.*, top-right plot at 55 mm) from shock reflection off sylgard/Ta interface and a secondary rarefaction (*e.g.*, bottom-left plot around 55 mm) from reflection off the outter surface of Ta wall. The distance behind the detonation front of the secondary shock in-

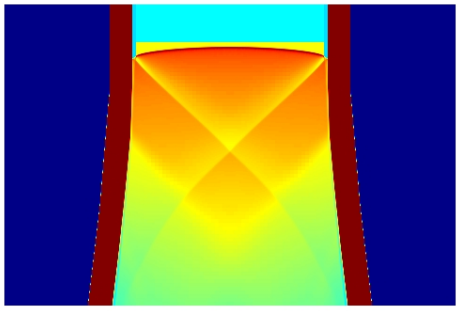

Figure 12: Density plot showing detonation wave in donor just before impact with barrier. Dark red corresponds to tantalum wall.

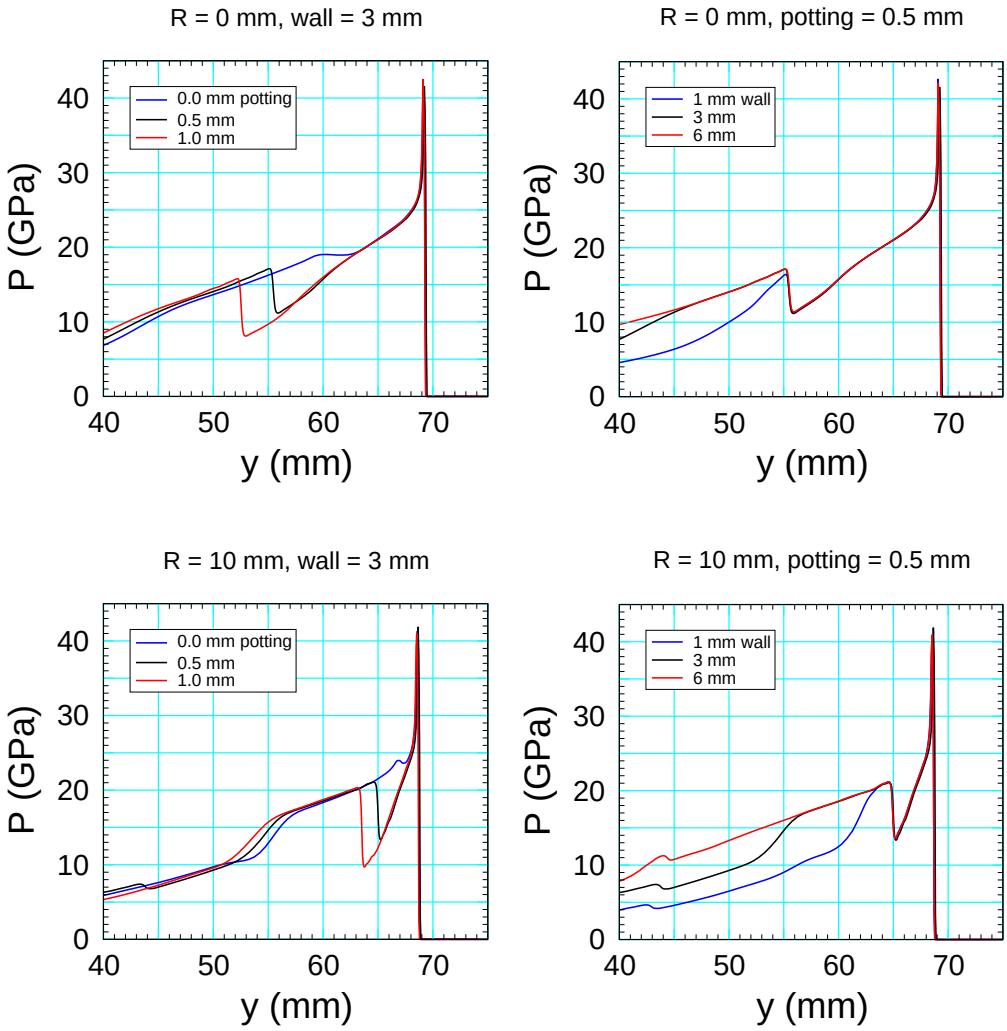

Figure 13: Pressure profile of detonation wave in donor. Top and bottom plots show variation with radius; centerline and near wall, respectively. Left and right plots show variation with potting layer thickness and wall thickness, respectively.

creases with the distance from the wall. Hence, it is largest on the centerline. In addition, the distance increase with the thickness of the sylgard layer, but not the wall thickness. Behind the secondary shock, the profiles near the wall display a secondary rarefaction. This rarefaction is too far behind to see in the profiles on the centerline. The wall thickness affects how far the secondary rarefaction is behind the shock.

In contrast to the rate stick, the pressure is not always largest on the centerline. Therefore, if the acceptor detonates, the ignition point may not be on the centerline. For the simulations in this section, the experimental slab confinement parameters are used. A comparison of the donor detonation wave profiles for the slab and cylindrical geometries are shown in figure 14. Since the slab configuration is more heavily confined, the pressure behind the detonation front falls off more slowly. The pressure falls below the 8 GPa ignition shock threshold on the Pop plot at a much larger distance for the slab; 22 to 28 mm for the slab vs 14 mm for the rate stick. Therefore, the barrier threshold thickness is expected to be significantly larger for the slab experiments.

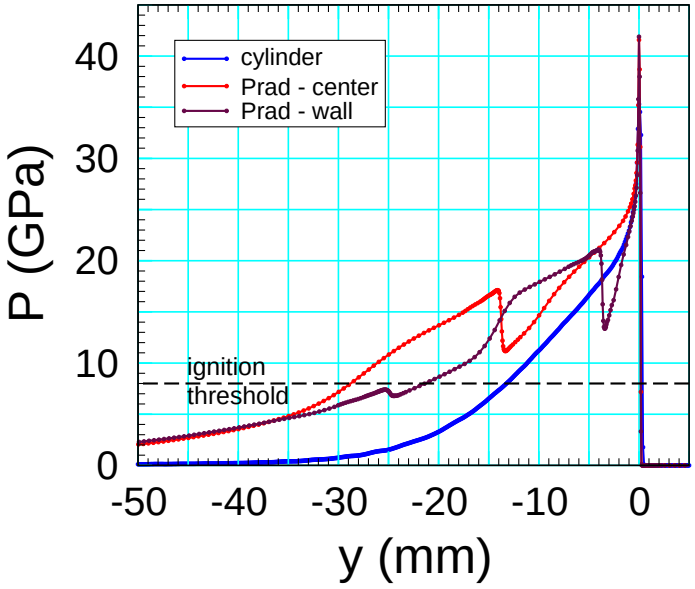

Figure 14: Comparison of detonation wave profiles for slab (3 mm Ta and 0.5 mm silgard) and cylindrical geometry.

4.1 Inert acceptor

To illustrate the effect of the slower fall off in the pressure behind the donor detonation wave, we simulate the case of a 35 mm solid epoxy barrier ($70 < y < 105$ mm) with an inert acceptor. Pressure profiles along the centerline and near the wall for the initial match of the donor detonation wave into the epoxy are shown in figure 15.

At the earlier time, $t = 12.8$, the pressure profile shows 2 waves in the donor. The right facing secondary shock from the reflection off the wall, and a left facing rarefaction wave from the match with the epoxy. Later,

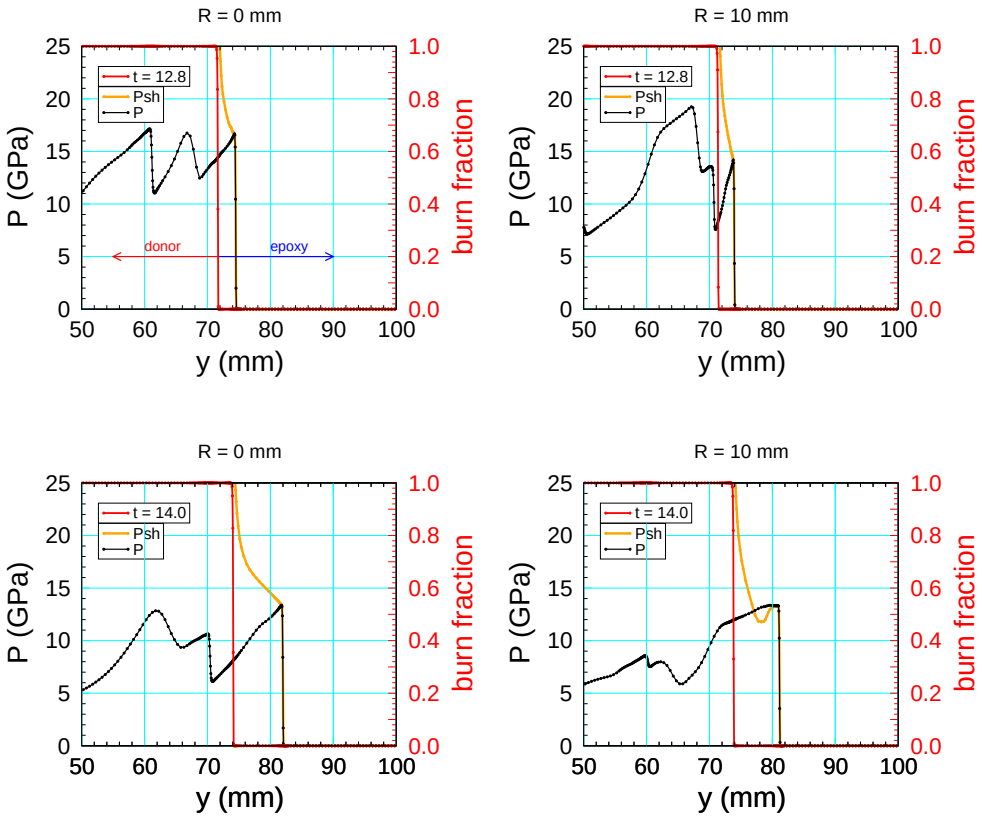

Figure 15: Barrier experiment with 35 mm epoxy barrier. Profiles of pressure and lead shock pressure showing initial shock match of detonation wave into the epoxy. The abrupt falloff in the burn fraction marks the end of the donor. Left and right columns correspond to profiles along centerline and near wall, respectively.

$t = 14.0$, the left facing wave has past through the secondary shock. On the centerline, the secondary shock is near the epoxy interface. Near the wall, the secondary shock has impacted the epoxy and causes the lead shock pressure in the epoxy to reverse its decay and start increasing. In general, the time and axial position at which the secondary shock catches up to the lead shock will depend on the distance from the wall.

The evolution of the pressure profiles in the epoxy is shown in figure 16. Two points to note are: i. The lead shock pressure is not monotonically decreasing with distance of propagation. ii. The shock pressure is not always greatest on the centerline. Both complications result from the secondary shock in the donor.

Pressure profiles of the match of the epoxy shock into the (inert) acceptor are shown in figure 17. The shock pressure in the epoxy before impact and the initial acceptor shock pressure are both about the same as shown in figure 6 for the rate stick with the 10 mm barrier, despite the much larger barrier thickness. This is due to the difference in the pressure profiles behind the donor detonation wave, see figure 14.

The lead shock pressure in the (inert) acceptor does not fall below the shock threshold pressure on the Pop plot of 8 GPa until the shock has traveled about 25 mm into the acceptor. This is much larger than for the rate stick case. The difference is partly due to the pressure profile behind the donor detonation wave. An additional contributing factor is that with the increased thickness of the epoxy barrier, a rarefaction wave spreads out and the pressure gradient decreases. Hence, the decay of the shock in the acceptor is slower.

With a reaction model, a 35 mm thick epoxy barrier is below the threshold thickness and the acceptor detonates. The pRad experiments used other types of barriers with shorter predicted threshold thicknesses; see [Dattelbaum et al., 2015]. With a 5 mm Ta barrier the acceptor did not detonate. Tantalum has a much higher density than epoxy; a factor of 14. Hence, a 5 mm Ta barrier has twice the mass of a 35 mm epoxy barrier. It also has a stiffer EOS which affects the impedance matches; see figures 2 and 3.

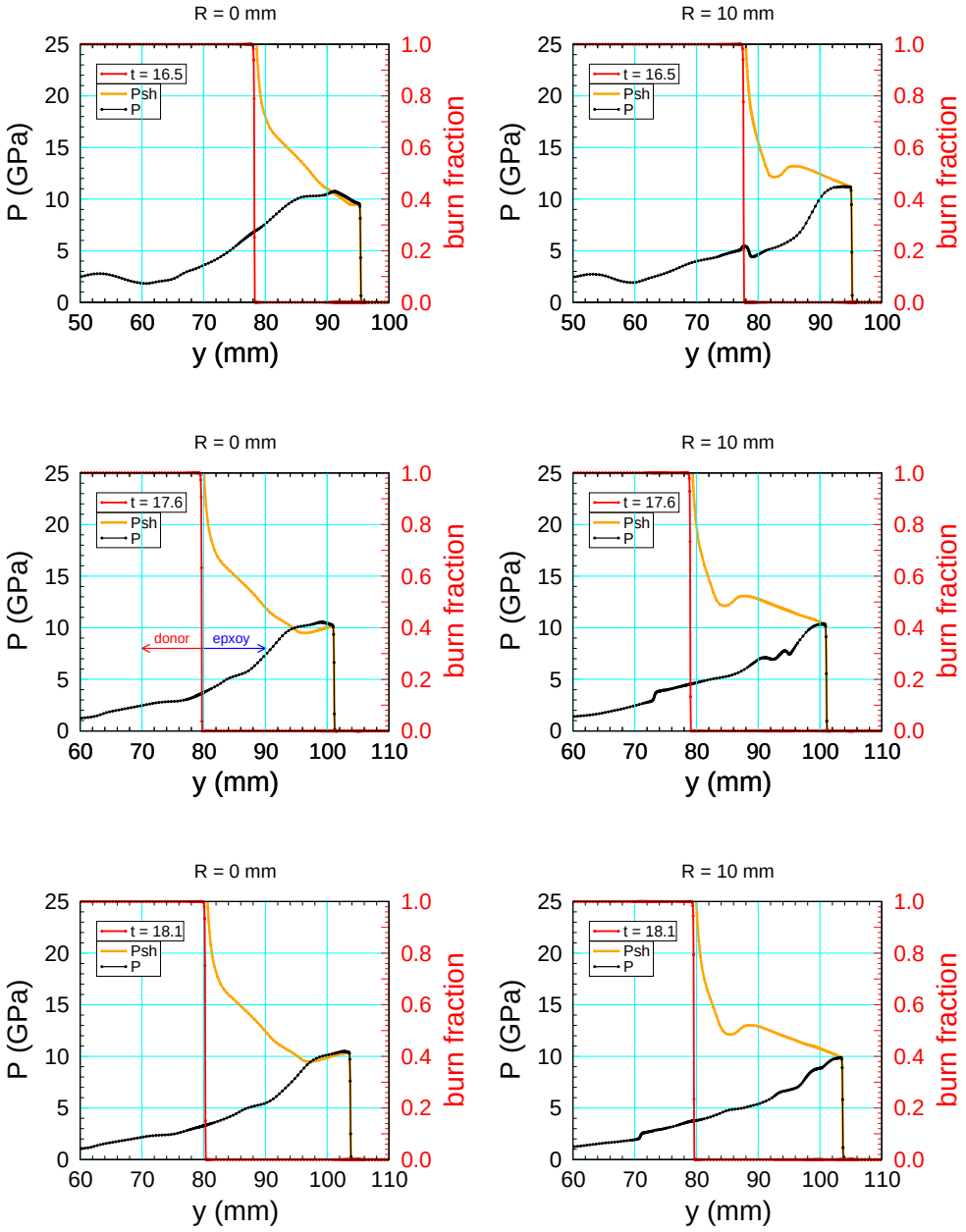

Figure 16: Barrier experiment with 35 mm epoxy barrier. Time evolution of profiles of pressure and lead shock pressure as shock propagates through the epoxy. The abrupt falloff in the burn fraction marks the end of the donor. Left and right columns correspond to profiles along centerline and near wall, respectively.

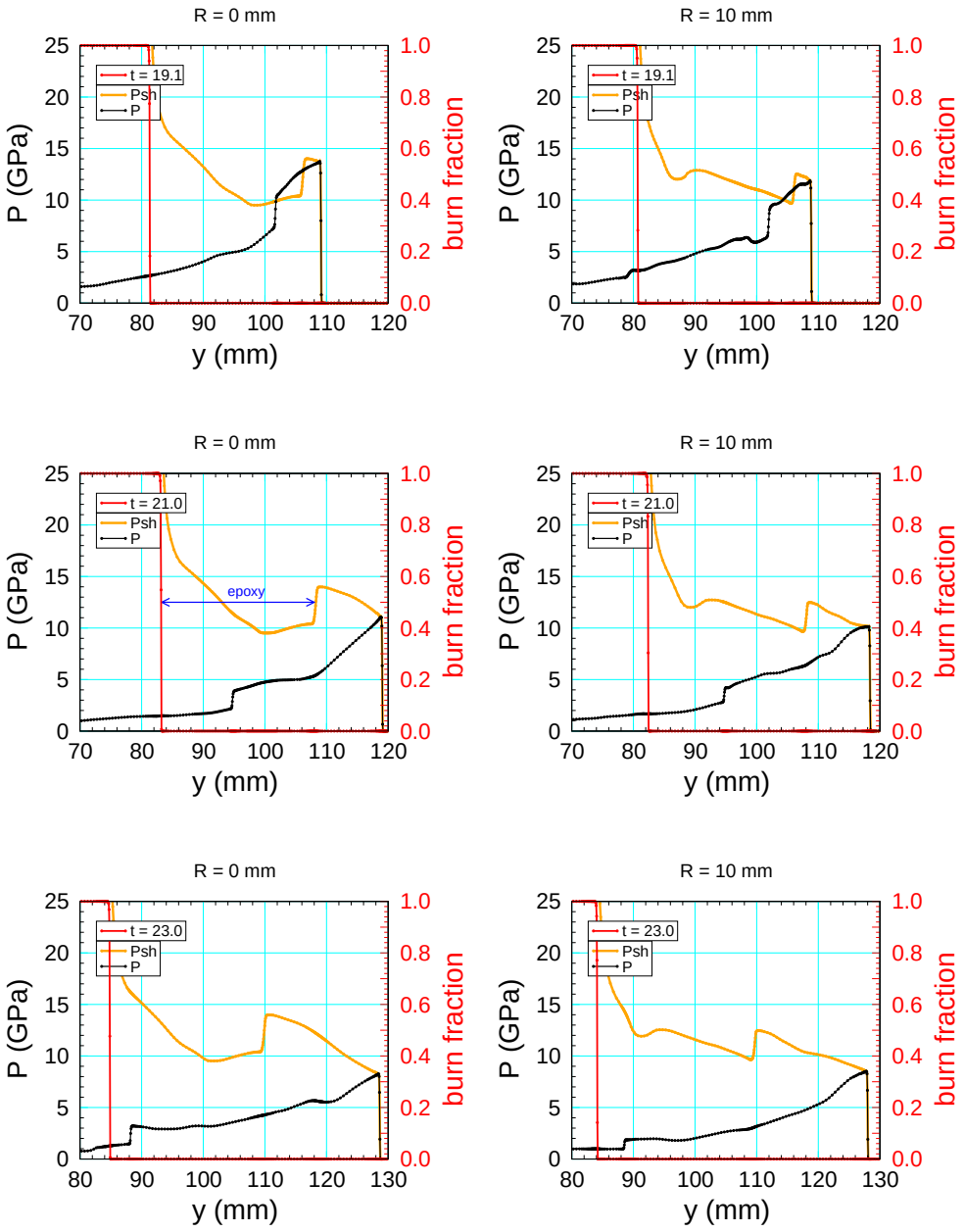

Figure 17: Barrier experiment with 35 mm epoxy barrier. Time evolution of profiles of pressure and lead shock pressure as shock propagates into the (inert) acceptor. The abrupt falloff in the burn fraction marks the end of the donor. The jump in shock pressure (around $y = 105$ to 110 mm) marks the end of the epoxy. Left and right columns correspond to profiles along centerline and near wall, respectively.

5 Summary

Simulations of the barrier experiments illustrate three factors that affect shock initiation under complex loading conditions:

1. Impedance matches.
   Shock match from the barrier material to the acceptor HE.

2. Shock decay.
   Strength of the lead shock wave in the acceptor decreases due to the pressure gradient behind the shock front and due to divergence of the shock from the curvature of the front.

3. Competition with burn rate.
   The burn rate increases the pressure leading to a pressure gradient that strengthens the lead shock. The competition between the burn rate and factors leading to shock decay determine whether or not a transition-to-detonation occurs.

There is an additional factor that has not been discussed. The loading of some barrier material can generate weak precursors ahead of the main wave impacting the acceptor. The precursor can be either due to elastic-plastic material response or due to non-uniformities such as for a perforated barrier. A weak shock wave can lead to shock desensitization of the acceptor HE. This has the effect of increasing the time for the pressure gradient from a rarefaction wave to catch up with and weaken the lead shock in the acceptor. The effect is similar to having a thicker barrier.

Precursors increase the difficulty of the simulations. Elastic-plastic behavior requires more advance material models. With the perforated barrier, the flow in the barrier and acceptor becomes three-dimensional. Cylindrical barrier experiments have shown that precursors do decrease the barrier threshold [Francois and Scovel, 2014]. Modeling precursors and shock desensitization are beyond the scope of this report.

Acknowledgements

Christina Scovel and Erik Moro have also performed simulations of the barrier experiments. Comparison with their results has been very helpful.

References

T. D. Aslam, R. L. Gustavsen, and B. D. Bartram. An equation of state for polyurea aerogel based on multi-shock response. *Journal of Physics: Conference Series*, 500:032001, 2014. URL http://dx.doi.org/10.1088/1742-6596/500/3/032001. 4

D. Dattelbaum, R. Gustavsen, S. Jackson, R. Menikoff, E. Moro, and C. Scovel. Prad barrier postshot report. Technical report, Los Alamos National Lab., 2015. LA-CP-15-20581. 2, 20

E. G. Francois and C. A. Scovel. Investigations of PBX 9502 relight phenomena using a modified gap test: Part 1, 2014. URL http://permalink.lanl.gov/object/tr?what=info:lanl-repo/lareport/LA-UR-14-21545. Presentation at conference Shock Compression in Condensed Matter. 2, 23

T. R. Gibbs and A. Popolato, editors. *LASL Explosive Property Data*. Univ. of Calif. Press, 1980. URL http://lib-www.lanl.gov/ladcdmp/epro.pdf. 2, 3

C. L. Mader. *Numerical Modeling of Explosives and Propellants*. CRC Press, 3rd edition, 2007. 8

R. Menikoff and M. S. Shaw. Review of the Forest Fire model for high explosives. *Combustion Theory and Modelling*, 12:569–604, 2008. URL http://dx.doi.org/10.1080/13647830801942402. 8

R. Menikoff and M. S. Shaw. Reactive burn models and ignition & growth concept. *EPJ Web of Conferences*, 10, 2010. doi: 10.1051/epjconf/20101000003. URL http://www.epj-conferences.org/articles/epjconf/pdf/2010/09/epjconf_nmh2010_00003.pdf. 8

G. B. Whitham. *Linear and Nonlinear Waves*. John Wiley & Sons, 1974. 8